Direct Observation of Charge Inversion by Multivalent Ions as a Universal Electrostatic Phenomenon

K. Besteman, M. A. G. Zevenbergen, H. A. Heering, and S. G. Lemay
Kavli Institute of Nanoscience, Delft University of Technology, 2628 CJ Delft, The Netherlands
(Received 26 April 2004; published 20 October 2004)

We have directly observed reversal of the polarity of charged surfaces in water upon the addition of trivalent and quadrivalent ions using atomic force microscopy. The bulk concentration of multivalent ions at which charge inversion reversibly occurs depends only very weakly on the chemical composition, surface structure, size, and lipophilicity of the ions, but is very sensitive to their valence. These results support the theoretical proposal that spatial correlations between ions are the driving mechanism behind charge inversion.

DOI: 10.1103/PhysRevLett.93.170802 PACS numbers: 07.79.Lh, 61.20.Qg, 82.45.Gj

Understanding screening due to mobile ions in liquid is a key theme of such diverse fields as polymer physics, nanofluidics, colloid science, and molecular biophysics. Several counterintuitive phenomena occur at high concentrations of multivalent ions. Examples include attraction between like-charged macromolecules such as DNA [1] or actin filaments [2] and reversal of the sign of the electrophoretic mobility of charged colloids [3,4]. The latter effect has become known as charge inversion.

The conventional paradigm for describing screening in liquid divides the screening ions into two components: (i) the so-called Stern layer, consisting of ions confined to the surface, and (ii) a diffuse component described by the Poisson-Boltzmann (PB) equation that decays exponentially with distance far from the charged object. Charge inversion can be accounted for by introducing a ''chemical'' binding constant that reduces the free energy of multivalent ions situated in the Stern layer, reflecting an assumed specific interaction between these ions and the surface being screened. This binding constant is expected to depend on properties of the ions such as their size, chemical composition, surface structure, lipophilicity, and valence. While this approach has been successful in *describing* experimental data [3,5–7], it usually provides little insight into the underlying binding mechanism and lacks significant predictive power.

A universal mechanism for charge inversion based predominantly on electrostatic interactions has been proposed [8]. It was noted that the predicted chemical potential of the Stern layer can be significantly lowered if spatial correlations between discrete ions are accounted for. At room temperature, the loss of entropy entailed by the formation of a highly correlated ionic system is substantial. For multivalent counterions and sufficiently high surface charge densities, however, this is more than compensated by the corresponding gain in electrostatic energy, leading to charge inversion [9]. To date, these theories have remained untested by experiments.

Here we present direct measurements of charge inversion and its dependence on the properties of the screening ions. Using an atomic force microscope (AFM), we measured the force between two oppositely charged surfaces. This approach circumvents the main limitations of previous measurements, namely, reliance on modeling of hydrodynamic effects [3,4] and the need to disentangle phenomena at two similarly charged surfaces [5,7]. We observe that in the presence of a sufficiently high concentration of trivalent and quadrivalent ions, the force reversibly changes sign. The bulk concentration at which charge inversion occurs, c_0, depends almost exclusively on the valence of the ions, consistent with the universal predictions of ion-correlation theories.

Positively charged amine-terminated surfaces were prepared under argon atmosphere by immersing silicon wafers with 200–500 nm thermally grown oxide in a 0.1% solution of 1-trichlorosilyl-11-cyanoundecane (Gelest) in toluene for 30 min, then in a 20% solution of Red Al (Sigma-Aldrich) in toluene for 5 h. Negatively charged surfaces were prepared by gluing 10 μm diameter silica spheres (G. Kisker Gbr) with epoxy resin to AFM cantilevers (ThermoMicroscope Microlevers, nominal force constant 0.03 N/m) using the method of Ducker *et al.* [10], as illustrated in Fig. 1(a). Force spectroscopy measurements were performed using a Digital Instrument NanoScope IV AFM to yield the force F on the silica bead versus the bead-surface separation d [10].

At separations d greater than the Debye length λ of the solution, the force F decays exponentially with d:

$$F = F_0 \exp(-d/\lambda), \qquad d > \lambda. \tag{1}$$

The parameter F_0 is proportional to the so-called renormalized surface charge densities of both the silica bead and the amine-terminated surface, $\sigma_b^\star$ and $\sigma_s^\star$, respectively. The values of $\sigma_{b,s}^\star$ are related by the PB equation to the net surface charge densities σ_b and σ_s (including both the bare surface charge and the charge in the Stern layer). At low net surface charge densities $|\sigma_{b,s}| < \sigma_{\max}$, the renormalized charge densities are simply equal to the net charge densities: $\sigma_{b,s}^\star = \sigma_{b,s}$. Here $\sigma_{\max} \approx 4kT\epsilon/e\lambda$, where k is the Boltzmann constant, T is the

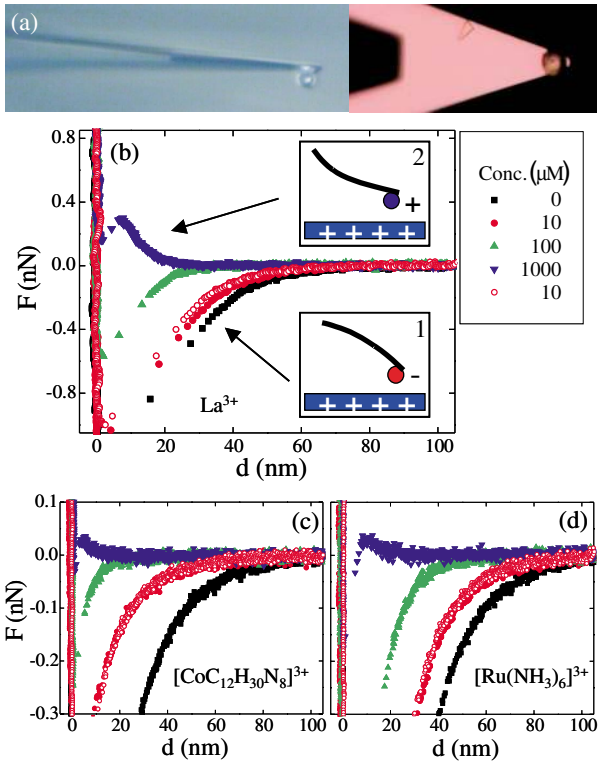

FIG. 1 (color). (a) Optical microscope images of the side (left) and top (right) of a cantilever with a silica sphere. Force versus separation measurements in different concentrations of (b) $LaCl_3$, (c) $CoC_{12}H_{30}N_8Cl_3$, and (d) $Ru(NH_3)_6Cl_3$. The insets illustrate schematically the attractive (1) and repulsive (2) forces between the silica bead and the amine-terminated surface. The legend applies to all three graphs.

temperature, ϵ is the dielectric constant of water, and $-e$ is the electron charge. At higher net charge densities, $\sigma^{\star}_{b,s}$ saturates at $\sigma_{\max}$. Because we use oppositely charged surfaces and Z:1 electrolytes, where Z is the valence of the multivalent ions, correlation effects are relevant only at one of the surfaces. The other surface can thus be thought of as a constant probe [11]. Near charge inversion, F_0 is approximately proportional to the net surface charge density of the surface being screened by multivalent ions, σ_b or σ_s, and the sign of the force unambiguously yields the polarity of this net surface charge.

For $d \lesssim \lambda$, the PB equation predicts a more complicated form than Eq. (1). van der Waals forces, regulation of the surface charge, and depletion forces can also become important. We therefore concentrate our analysis on the regime where both $d > \lambda$ and van der Waals forces are small ($d > 10$ nm), where we can reliably fit to Eq. (1).

Three positive trivalent ions were investigated. Lanthanum La^{3+} is a metal ion with a first hydration shell consisting of 8–9 water molecules (radius r of the complex 398 pm [12–15]). Ruthenium(III) hexammine $[Ru(NH_3)_6]^{3+}$ contains a Ru(III) core surrounded by six NH_3 groups ($r = 364$ pm [12–14]). Cobalt(III) sepulchrate $[CoC_{12}H_{30}N_8]^{3+}$ is a caged cobalt complex with CH_2 groups exposed to the solvent ($r = 445$ pm [16]), making it less hydrophilic than the other two.

Figure 1 shows the measured force-distance relation $F(d)$ as a function of multivalent ion concentration c for the multivalent salts $LaCl_3$ (b), $CoC_{12}H_{30}N_8Cl_3$ (c), and $Ru(NH_3)_6Cl_3$ (d). A force measurement with only a supporting electrolyte ($LaCl_3$: [17]; $CoC_{12}H_{30}N_8Cl_3$ and $Ru(NH_3)_6Cl_3$: [18]) was first performed (black squares), showing an attractive interaction between the surfaces. Solutions with increasing concentrations of multivalent ions in addition to the monovalent supporting electrolyte were then pumped through the AFM fluid cell of 50 μl volume at a rate 0.15–0.2 ml/min for at least 5 min per solution. This allowed the surface to equilibrate with the bulk electrolyte and ensured that c was not diminished by ions screening the surface. Consecutive measurements of $F(d)$ at multivalent ion concentrations $c = 10$ μM, 100 μM, and 1 mM are shown in Fig. 1. At the end of the experiment, the measurement with $c = 10$ μM was repeated (red open circles). The $CoC_{12}H_{30}N_8Cl_3$ and $Ru(NH_3)_6Cl_3$ measurements were carried out consecutively using the same silica bead.

We interpret these observations as follows. The positive multivalent ions adsorb on the negative silica bead, reducing σ_b and thus the magnitude of the force. Near 1 mM, the screening charge in the Stern layer overcompensates for the bare surface charge; σ_b becomes positive and the force becomes repulsive. The last measurement with $c = 10$ μM, which shows a recovery to the force measured at the beginning of the experiment, indicates that charge inversion reflects reversible equilibrium between the surface and the bulk electrolyte.

We fitted each $F(d)$ curve to Eq. (1) for $d > \lambda$. Because it is difficult to accurately fit λ when the force is very small, its value was fitted for the curve with $c = 0$ [e.g., $\lambda = 18$ nm for the data of Figs. 1(c) and 1(d)] and corrected using the standard expression for λ when $c > 0$ [e.g., $\lambda = 4$ nm for the 1 mM data in Figs. 1(c) and 1(d)].

Figure 2(a) shows the fitted normalized force extrapolated to zero separation, $F_{N0}(c) = F_0(c)/F_0(0)$, for the

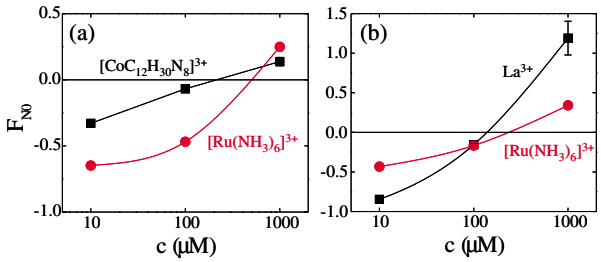

FIG. 2 (color online). Normalized force extrapolated to zero separation obtained from fits to Eq. (1), versus multivalent ion concentration c for (a) $CoC_{12}H_{30}N_8Cl_3$ (squares) and $Ru(NH_3)_6Cl_3$ (circles) and for (b) $LaCl_3$ (squares) and $Ru(NH_3)_6Cl_3$ (circles). In each case the data were obtained consecutively using the same silica bead. Lines are guides to the eye.

TABLE I. Summary of measurements in which the same surface was charge inverted by two different ions.

Surface	Probe	Supp. elect.	Ion(1)	Ion(2)	$c_0^{(1)}$ (μM)	$c_0^{(2)}$ (μM)	$c_0^{(high)}/c_0^{(low)}$
Chlorosilane	Silica bead	[19]	$[Fe(CN)_6]^{4-}$	$[Fe(CN)_6]^{3-}$	4	200	50
Chlorosilane	Silica bead	[19]	$[Fe(CN)_6]^{4-}$	$[Fe(CN)_6]^{3-}$	6	450	75
APTES	Silica bead	[20]	$[Fe(CN)_6]^{4-}$	$[Fe(CN)_6]^{3-}$	13	170	13
APTES	Silica bead	[20]	$[Ru(CN)_6]^{4-}$	$[Fe(CN)_6]^{4-}$	11	13	1.2
Silica bead	APTES	[20]	La^{3+}	$[Ru(NH_3)]^{3+}$	560	730	1.3
Silica bead	Poly-L-lysine	[17]	$[CoC_{12}H_{30}N_8]^{3+}$	La^{3+}	190	120	1.6
Silica bead	Poly-L-lysine	[17]	$[CoC_{12}H_{30}N_8]^{3+}$	La^{3+}	170	180	1.1
Silica bead	Chlorosilane	[17]	La^{3+}	$[Ru(NH_3)]^{3+}$	130	210	1.6
Silica bead	Chlorosilane	[18]	$[CoC_{12}H_{30}N_8]^{3+}$	$[Ru(NH_3)]^{3+}$	210	450	2.1
Poly-L-lysine	Silica bead	[20]	$[Ru(CN)_6]^{4-}$		22		

$[CoC_{12}H_{30}N_8]^{3+}$ and $[Ru(NH_3)_6]^{3+}$ data of Figs. 1(c) and 1(d). Similarly, Fig. 2(b) shows $F_{N0}(c)$ for consecutive measurements using the same silica bead on La^{3+} [data from Fig. 1(b)] and $[Ru(NH_3)_6]^{3+}$ ($F(d)$ curves not shown). We estimate the charge-inversion concentration c_0 by linearly interpolating between the data points immediately above and below $F_N = 0$ on the lin-log scale. In both sets of measurements, the observed values of c_0 differ by a factor of $\sim$2. More generally, we find that the charge-inversion concentrations of silica for the three chemically different trivalent ions La^{3+}, $[Ru(NH_3)_6]^{3+}$ and $[CoC_{12}H_{30}N_8]^{3+}$ differ by at most a factor of 2.1, as summarized in Table I. This is comparable to the variation observed between measurements for the same ion and pH using different, nominally identical beads and surfaces. Although the charge-inversion concentrations of the three positive trivalent ions are similar, there are differences in the observed $F(d)$ curves. In particular, La^{3+} is less effective in reducing the absolute force at low concentrations, but it exhibits the largest magnitude of the force for $c \gg c_0$.

Figure 3 shows measurements where the same amine-terminated surface was consecutively charge inverted by a molecule in two different charge states, iron(II) hexacyanide $[Fe(CN)_6]^{4-}$ ($r = 443$ pm) and iron(III) hexacyanide $[Fe(CN)_6]^{3-}$ ($r = 437$ pm) [12–14], ensuring that essentially the only difference between the two measurements is the valence of the ions. Figure 3(c) shows F_{N0} versus c for both ions [19]. The charge-inversion concentrations for the two ions differ by a factor of $\sim$50.

Measurements using $[Fe(CN)_6]^{4-}$ and ruthenium(II) hexacyanide $[Ru(CN)_6]^{4-}$ ($r = 456$ pm [12–14]), two ions with the same chemical groups exposed to solution and differing only by their core atom, gave nearly identical $F(d)$ curves at all concentrations.

Two divalent ions, Ca^{2+} and Mg^{2+} [15], did not show charge inversion at a concentration of 1 mM on a silica bead that showed charge inversion at 1 mM La^{3+}. Thus divalent ions, if they can charge invert a silica bead at all, do so at higher concentrations than trivalent ions. Concentrations higher than 1 mM were not investigated because λ then becomes so short that other effects mask the electrostatic interaction between the surfaces.

Additional experiments were performed with positively charged surfaces made by chemically modifying a silicon dioxide surface with 3-aminopropyltriethoxysilane (APTES) and by adsorbing poly-L-lysine on mica. The main results are summarized in Table I

In terms of a chemical binding description, our measurements indicate that the binding constants for La^{3+}, $[Ru(NH_3)_6]^{3+}$, and $[CoC_{12}H_{30}N_8]^{3+}$ on silica differ by at most a factor of $\sim$2, despite the fact that these ions have significantly different chemical composition, surface structure, size, and lipophilicity. The binding constant differs by more than a factor of 10 for the same molecule in two different charge states on amine-terminated surfaces. These observations strongly suggest that specific chemical interactions are not responsible for charge in-

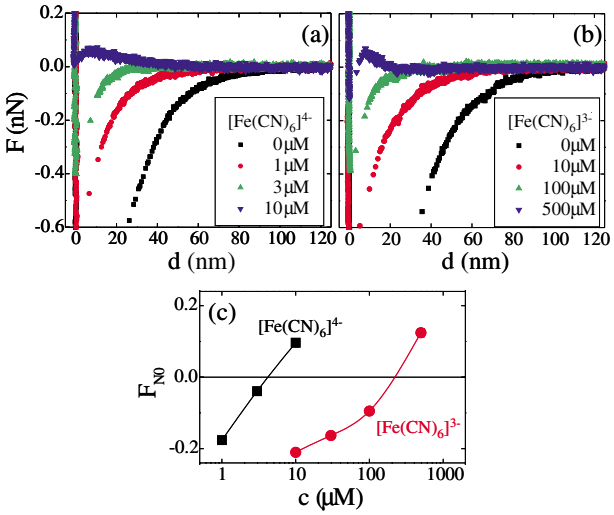

FIG. 3 (color). Force versus separation measurements in different concentrations of (a) $K_4Fe(CN)_6$ and (b) $K_3Fe(CN)_6$. (c) Normalized force at zero separation versus multivalent ion concentration c for $K_4Fe(CN)_6$ (squares) and $K_3Fe(CN)_6$ (circles). Lines are guides to the eye.

version in our measurements and that the mechanism for adsorption is predominantly electrostatic.

We compare our results with ion-correlation theories using the formalism of Shklovskii [9], in which the multivalent counterions in the Stern layer are assumed to form a strongly correlated liquid with short-range correlations resembling those of a Wigner crystal. This theory provides a simple analytical prediction for c_0:

$$c_0 = (\sigma_{\text{bare}}/2erZ)\exp(-|\mu_c|/kT)\exp(\Delta\mu^0/kT). \quad (2)$$

Here σ_{bare} is the bare surface charge density, $\Delta\mu^0$ is the standard energy of adsorption of an ion, and μ_c is the chemical potential of the strongly correlated liquid. The latter can be approximated by the value for a Wigner crystal: $\mu_c \propto \sigma_{\text{bare}}^{1/2} Z^{3/2}$. In the calculations we use the full expression for μ_c [9].

In the absence of hydration effects and specific chemical interactions, $\Delta\mu^0 = 0$ and μ_c is solely responsible for charge inversion. In this case charge- inversion is a universal electrostatic effect and c_0 depends very sensitively on Z but is independent of the chemical structure of the ions. This is in good qualitative agreement with our observations.

Equation (2) has two unknowns, σ_{bare} and $\Delta\mu^0$, which can be deduced from consecutive measurements using $[Fe(CN)_6]^{4-}$ and $[Fe(CN)_6]^{3-}$ on the same surface. From rows 1 and 2 in Table I we extract values of $\sigma_{\text{bare}} = +0.45$ and $+0.55e/\text{nm}^2$, and $\Delta\mu^0 = -1.4kT$ and $-0.1kT$, respectively. The calculation assumes that $\Delta\mu^0$ and σ_{bare} are the same for both measurements. The corresponding values of $|\mu_c|$ are $9.4kT$ and $10.6kT$ for $Z = 4$ and $5.8kT$ and $6.5kT$ for $Z = 3$. The observation that $|\mu_c| \gg |\Delta\mu^0| \lesssim kT$ indicates that specific interactions are negligible and that ion correlations are the dominant mechanism behind charge inversion in this system.

The same calculation for the APTES measurements in Table I (row 3) yields $\sigma_{\text{bare}} = +0.2e/\text{nm}^2$, $\Delta\mu^0 = -3.0kT$, and $|\mu_c| = 5.8kT$ and $3.5kT$ for $Z = 4$ and 3, respectively. This suggests that specific adsorption plays a larger role in this case. However, the value of μ_c for APTES and $Z = 3$ corresponds to the lower end of the range of validity of Eq. (2) [9], which may be responsible for the difference. In addition, the surface charge was modeled as being uniformly distributed, whereas real surfaces consist of discrete chemical groups. This disorder is expected to facilitate charge inversion [9], and its relative importance should be greater for APTES with its smaller σ_{bare}. Elucidating the interplay between disorder and correlations remains an important theoretical challenge.

Taking $\Delta\mu^0 = 0$ and $c_0 = 200\ \mu\text{M}$ for $[CoC_{12}H_{30}N_8]^{3+}$ screening silica gives $\sigma_{\text{bare}} = -0.75e/\text{nm}^2$, consistent with commonly accepted values [21].

These experiments are among the first systematic steps toward understanding the fundamentals of screening of real surfaces by multivalent ions. Specific binding does not provide an adequate explanation for our observations. An alternative description based on ion correlations yields qualitative and semiquantitative agreement.

We thank J. Lyklema for useful discussions and C. Dekker for general support and useful discussions. This work was supported by FOM and NWO.

[1] V. A. Bloomfield, Biopolymers **44**, 269 (1998).
[2] T. E. Angelini *et al.*, Proc. Natl. Acad. Sci. U.S.A. **100**, 8634 (2003).
[3] R. O. James and T. W. Healey, J. Colloid Interface Sci. **40**, 42 (1972); **40**, 53 (1972); **40**, 65 (1972).
[4] A. Martín-Molina *et al.*, J. Chem. Phys. **118**, 4183 (2003).
[5] R. M. Pashley, J. Colloid Interface Sci. **102**, 23 (1984).
[6] K. B. Agashe and J. R. Regalbuto, J. Colloid Interface Sci. **185**, 174 (1996).
[7] V. Vithayaveroj, S. Yiacoumi, and C. Tsouris, J. Disp. Sci. Technol. **24**, 517 (2003).
[8] For comprehensive reviews, see A. Yu. Grosberg, T. T. Nguyen, and B. I. Shklovskii, Rev. Mod. Phys. **74**, 329 (2002); Y. Levin, Rep. Prog. Phys. **65**, 1577 (2002); M. Quesada-Pérez *et al.*, Chem. Phys. Chem. **4**, 234 (2003).
[9] B. I. Shklovskii, Phys. Rev. E **60**, 5802 (1999).
[10] W. A. Ducker, T. J. Senden, and R. M. Pashley, Langmuir **8**, 1831 (1992).
[11] The value of $\sigma^\star \approx \sigma_{\text{max}}$ for the probe is not really constant since it depends linearly on λ^{-1} and more subtly on the valence of the coions; G. Téllez and E. Trizac, Phys. Rev. E **70**, 011404 (2004). This has no influence on the measured sign of the force, however, and the error induced in c_0 is of the same order as that from other sources.
[12] Sum of metal ion radius and ligand (H_2O, NH_3, CN^-) diameter. Agrees within 4% with crystallographic data.
[13] R. D. Shannon, Acta Crystallogr. Sect. A **32**, 751 (1976).
[14] Y. Marcus, *Ion Properties* (Marcel Dekker Inc., New York, 1997), Chap. 3.
[15] All measurements were done at *p*H less than the first hydrolysis constant of the ions; J. Burgess, *Metal Ions in Solution* (Ellis Horwood, Chichester, England, 1979).
[16] Crystal structure with van der Waals radii; A. Bacchi, F. Ferranti, and G. Pelizzi, Acta Crystallogr. Sect. C **49**, 1163 (1993).
[17] The supporting electrolyte was a 1 mM HEPES (4-(2-hydroxyethyl)piperazine-1-ethanesulfonic acid) buffer, *p*H 7.0 ± 0.3 set by adding KOH.
[18] The supporting electrolyte was a mixture of 0.3 mM KOH and HCl with *p*H 6.5 ± 0.5.
[19] The supporting electrolyte was the same as [18] with *p*H 5.8 ± 0.3.
[20] The supporting electrolyte was a 0.1 mM MES (2-morpholinoethanesulfonic acid) buffer, *p*H 6.0 ± 0.3 set by adding KOH.
[21] R. K. Iler, *The Chemistry of Silica* (Wiley, New York, 1979).